ACADEMIC STUDIES IN SCIENCE AND MATHEMATICS

EDITOR:

PROF. TURGAY SEÇKİN, PH.D.

gece kitaplığı

İmtiyaz Sahibi / Publisher • Yaşar Hız
Genel Yayın Yönetmeni / Editor in Chief • Eda Altunel
Editör / Editor • PROF. TURGAY SEÇKİN PH.D
Kapak & İç Tasarım / Cover & Interior Design • Karaf Ajans

Birinci Basım / First Edition • © MART 2020

ISBN • 978-625-7912-13-6

Gece Kitaplığı / Gece Publishing
Türkiye Adres / Turkey Address: Kızılay Mah. Fevzi Çakmak 1. Sokak
Ümit Apt. No: 22/A Çankaya / Ankara / TR
Telefon / Phone: +90 312 384 80 40
web: www.gecekitapligi.com
e-mail: gecekitapligi@gmail.com

Baskı & Cilt / Printing & Volume
Sertifika / Certificate No: 7083

Academic Studies in Science and Mathematics

EDITOR

PROF. TURGAY SEÇKİN PH.D

gece kitaplığı

CONTENTS

Chapter 1

ON FUZZY BERNSTEIN POLYNOMIALS

Esma Yıldız ÖZKAN[1]

1 Doç. Dr. Esma YILDIZ ÖZKAN, Gazi Üniversitesi, Fen Fakültesi, Matematik Bölümü

Bernstein polynomials were defined by Bernstein in order to prove the theorem of Weierstrass as follows

$$B_n(f;x) = \sum_{k=0}^{n} f\left(\frac{k}{n}\right) x^k (1-x)^{n-k}, \qquad x \in [0,1],$$

where f is a real valued function defined on $[0,1]$. Bernstein polynomials have been studied immensely in approximation theory.

Recently, significant results in approximation theory have been extended to fuzzy mathematics. The fuzzy Weierstrass approximation theorem with the applications was given firstly by Gal. Gal defined the fuzzy algebraic Bernstein polynomials and investigated its approximation properties [4,5,6,7].

In this study, we aim to obtain an approximation theorem including asymptotic expansions of Voronovskaja-type for the fuzzy Bernstein polynomials

Firstly, we introduce some notations in fuzzy mathematics. Secondly, we recall the concept of fuzzy Bernstein polynomial and its some fuzzy approximation properties. Finally, we investigate asymptotic expansions of Voronovskaja type for the fuzzy Bernstein polynomials.

Some Notations in Fuzzy Mathematics

Now, we recall the basic concepts of fuzzy mathematics. The details on this subject can be found deeply in [1,8,10,11,12,13].

Definition 1. If any function $u: \mathbb{R} \to [0,1]$ with the following properties

i. u is normal, i.e. there exists $x_0 \in \mathbb{R}$ such that $u(x_0) = 1$;

ii. u is a convex fuzzy set, i.e.

$$u(\lambda x + (1-\lambda)y) \geq min\{u(x), u(y)\}; x, y \in \mathbb{R}, \lambda \in [0,1];$$

iii. u is upper semi-continuous on $\mathbb{R}$, i.e. there exists at least a neighbor-hood $V(x_0)$ such that

$$u(x) \leq u(x_0) + \varepsilon, \forall x_0 \in \mathbb{R}, \forall \varepsilon > 0;$$

iv. $\overline{\{x \in \mathbb{R}: u(x) > 0\}}$ is compact in $\mathbb{R}$.

Then u is called a fuzzy number.

We denote the set of all fuzzy numbers defined above with $\mathbb{R}_{\mathcal{F}}$. If $u: \mathbb{R} \to [0,1]$ is a fuzzy number, then for all $0 \leq r < 1$, one can define

$$[u]^r = \begin{cases} \{x \in \mathbb{R}: u(x) \geq 0\}, & if\ 0 < r \leq 1, \\ \overline{\{x \in \mathbb{R}: u(x) > 0\}}, & if\ r = 0, \end{cases}$$

then $[u]^r$ is a closed and bounded interval of $\mathbb{R}$. On account of this characterization of fuzzy numbers, therefore a fuzzy number is determined completely by its end points u_-^r and u_+^r of the interval $[u]^r = [u_-^r, u_+^r]$.

Definition 2. For $u, v \in \mathbb{R}_{\mathcal{F}}$ and $k \in \mathbb{R}$, the addition and the scalar product are defined uniquely by
$[u+v]^r = [u]^r + [v]^r, [ku]^r = k[u]^r, r \in [0,1]$.

The addition and the scalar product are denoted by $u \oplus v$ and $k \odot u$ for $u, v \in \mathbb{R}_{\mathcal{F}}$, respectively.

Lemma 1. Let $k, l \in \mathbb{R}$, $w, z \in \mathbb{R}_{\mathcal{F}}$ and let $\tilde{o} = \chi_{\{0\}}$ be the characteristic function of $\{0\}$. Then

i. The neutral element with regard to $\oplus$ is $\tilde{o} \in \mathbb{R}$,

ii. For each $z \neq \tilde{o}, z \in \mathbb{R}_{\mathcal{F}}$ has any opposite in $\mathbb{R}_{\mathcal{F}}$,

iii. If $k, l > 0$ or $k, l \leq 0$, we have

$$(k+l) \odot z = k \odot z \oplus l \odot z,$$

$$k\odot(w\oplus z) = k\odot w\oplus k\odot z,$$

$$k\odot(l\odot z) = (k.l)\odot z.$$

Definition 3. If a function $D: \mathbb{R}_{\mathcal{F}} \times \mathbb{R}_{\mathcal{F}} \to \mathbb{R}_{+} \cup \{0\}$ .is defined by

$$D(u,v) = \sup_{r\epsilon[0,1]} max\{|u_{-}^{r} - u_{+}^{r}|, |u_{-}^{r} + u_{+}^{r}|\},$$

where $[u]^r = [u_{-}^{r}, u_{+}^{r}]$.and $[v]^r = [v_{-}^{r}, v_{+}^{r}]$ are closed and bounded intervals in $\mathbb{R}$ then D is a metric on $\mathbb{R}_{\mathcal{F}}$.

Theorem 1. $(\mathbb{R}_{\mathcal{F}}, D)$ is a complete metric space with the following properties

i. $D(u\oplus v, v\oplus w) = D(u,v), \forall u,v,w \in \mathbb{R}_{\mathcal{F}};$

ii. $D(k\odot u, k\odot u) = |k|D(u,v), \forall u,v \in \mathbb{R}_{\mathcal{F}}, k \in \mathbb{R};$

iii. $D(u\oplus v, w\oplus e) = D(u,w) + D(v,e), \forall u,v,w,e \in \mathbb{R}_{\mathcal{F}}.$

Definition 4. A partial order on $\mathbb{R}_{\mathcal{F}}$ is defined by $" \leq "$ such that $u \leq v$ for all $u,v \in \mathbb{R}_{\mathcal{F}}$ iff $[u]^r \leq [v]^r$ for all $u,v \in \mathbb{R}_{\mathcal{F}}$ and $r \in [0,1]$ iff $u_{-}^{r} \leq v_{-}^{r}$, $u_{+}^{r} \leq v_{+}^{r}$ for all $u,v \in \mathbb{R}_{\mathcal{F}}$ and $r \in [0,1]$.

Definition 5. Any function f from $I \subset \mathbb{R}$ to $\mathbb{R}_{\mathcal{F}}$ is called a fuzzy function.

Definition 6. The distance between two fuzzy functions f and g is defined by

$$D^*(f,g) = \sup_{x\epsilon I} D\big(f(x), g(x)\big).$$

Definition 7. Any fuzzy algebraic polynomial of degree *n* has the form

$$P_n(x) = \sum_{k=0}^{n} {}^{*}\, x^k \odot c_k,$$

where $c_k \epsilon \mathbb{R}_{\mathcal{F}}, k = 0,1,2, \dots, n$. Here $\sum^{*}$ denotes the finite fuzzy summation on $\mathbb{R}_{\mathcal{F}}$.

Definition 8. Let f be a fuzzy function defined on $I \subset \mathbb{R}$. If there exists that

$$\lim_{h \to 0} \frac{f(x+h) - f(x)}{h},$$

then we call the fuzzy function f differentiable at x and denoted by $f'(x)$. Analogously, the p-times derivatives $f^{(p)}(x)$ for $p \epsilon \mathbb{N}$ associated with a fuzzy function f can be defined.

Lemma 2. Suppose that f be a fuzzy function defined on $I \subset \mathbb{R}$ and be represented parametrically by

$$[f(x)]^r = [f_-^r(x), f_+^r(x)], \forall x \in I, \forall r \in [0,1],$$

where f_-^r and f_+^r are real valued function on *I*.

If f is p-times differentiable fuzzy function defined on I, then the corresponding real valued functions f_-^r and f_+^r are p-times differentiable on I for any $r \in [0,1]$., and that

$$[f^{(p)}(x)]^r = \left[\left(f^{(p)}\right)_-^r(x), \left(f^{(p)}\right)_+^r(x) \right], \forall x \in I, \forall r \in [0,1],$$

where $\left(f^{(p)}\right)_-^r$ and $\left(f^{(p)}\right)_+^r(x)$ are the corresponding p-times derivatives of $f_-^r(x)$ and $f_+^r(x)$, respectively.

Fuzzy Bernstein polynomials and its approximation properties

Gal defined the following fuzzy algebraic polynomial and investigated its approximation properties.

Definition 9. Let f be any fuzzy function defined on $[0,1]$. The fuzzy algebraic polynomial is defined by

$$B_n^{\mathcal{F}}(f;x)=\sum_{k=0}^{n}{}^{*}\binom{n}{k}x^k(1-x)^{n-k}\odot f\left(\frac{k}{n}\right), x\in[0,1].$$

Here $\sum^*$ and $\odot$ denote the finite fuzzy summation and the fuzzy scalar product $\mathbb{R}_{\mathcal{F}}$, respectively.

Let f be any fuzzy continuous function defined on $[0,1]$, mapping between the two metric spaces $([0,1],|.|)$ and $(\mathbb{R}_{\mathcal{F}},D)$. Let us denote with $C_{\mathcal{F}}[0,1]$ the set of all fuzzy continuous functions defined on $[0,1]$.

Definition 10. For any function $f\in C_{\mathcal{F}}[0,1]$, the first fuzzy modulus of continuity is defined by

$$\omega_1^{\mathcal{F}}(f;\delta)=\sup_{\substack{x,y\in[0,1]\\|x-y|\le\delta}}D\big(f(x),f(y)\big), \forall\delta>0.$$

Lemma 3. For any function $f\in C_{\mathcal{F}}[0,1]$ and $\delta>0$, the first fuzzy modulus of continuity $\omega_1^{\mathcal{F}}(f;\delta)$ satisfies the following properties

i. $\omega_1^{\mathcal{F}}(f;\delta_1+\delta_2)\le\omega_1^{\mathcal{F}}(f;\delta_1)+\omega_1^{\mathcal{F}}(f;\delta_2)$,

for all $\delta_1,\delta_2>0$;

ii. $\omega_1^{\mathcal{F}}(f;n\delta)\le n\omega_1^{\mathcal{F}}(f;\delta)$,

for all $\delta>0$ and $n\in\mathbb{N}$;

iii. $\omega_1^{\mathcal{F}}(f;n\lambda)\le(\lambda+1)\omega_1^{\mathcal{F}}(f;\delta)$,

for all $\delta,\lambda>0$;

iv. If $f\in C_{\mathcal{F}}[0,1]$ then $\lim_{\delta\to0}\omega_1^{\mathcal{F}}(f;\delta)=0$.

Gal gave the following the degree of the approximation.

Theorem 2. If $f \in C_{\mathcal{F}}[0,1]$, then

$$D\left(B_n^{\mathcal{F}}(f;x), f(x)\right) \leq \frac{3}{2}\omega_1^{\mathcal{F}}\left(f;\frac{1}{\sqrt{n}}\right), n\epsilon\mathbb{N}, x \in [0,1],$$

where $\omega_1^{\mathcal{F}}$ is the first fuzzy modulus of continuity.

Fuzzy Asymptotic Expansions

In this part, we give an approximation theorem including fuzzy asymptotic expansions of Voronovskaja type for the fuzzy Bernstein polynomials.

By $C_{\mathcal{F}}^2[0,1]$ be denoted the space of all fuzzy continuous functions defined on $[0,1]$ that are 2-times differentiable continuously on $[0,1]$.

Theorem 4. If $f \in C_{\mathcal{F}}^2[0,1]$ then

$$D\left(B_n^{\mathcal{F}}(f;x), f(x) \oplus \frac{1}{2} B_n((t-x)^2;x) \odot f''(x)\right)$$
$$\leq \frac{3}{2} D\left(\omega_1^{\mathcal{F}}\left(f;\frac{1}{\sqrt{n}}\right), \tilde{o}\right) + \frac{1}{8n} D^*(f'', \tilde{0}),$$

where $\tilde{o}$ is the neutral element with regard to $\oplus$ in $\mathbb{R}_{\mathcal{F}}$, $\tilde{0}$ is a fuzzy function defined on $[0,1]$ such that $\tilde{0}(x) = \tilde{o}$ for all $x \in [0,1]$ and $\omega_1^{\mathcal{F}}$ is the first fuzzy modulus of continuity.

Proof. Since $f \in C_{\mathcal{F}}^2[0,1]$, $[f(x)]^r$ is a bounded and closed in $\mathbb{R}$, which has the representation $[f(x)]^r = [f_-^r(x), f_+^r(x)]$ for all $x \in [0,1]$ such that f_-^r and f_+^r are in $C^2[0,1]$. Therefore $\|(f'')_-^r\|$ and $\|(f'')_+^r\|$ are bounded in $\mathbb{R}$.

For the classical Bernstein polynomial(see [2,3] for details), we have the following

$$B_n((\cdot - x)^2; x) = \frac{x(1-x)}{n} \leq \frac{1}{4n}, x \in [0,1] \tag{1}$$

and

$$\left|B_n(f_{\pm}^r; x) - f_{\pm}^r(x)\right| \leq \frac{3}{2}\omega_1\left(f_{\pm}^r; \frac{1}{\sqrt{n}}\right). \tag{2}$$

Here ω_1 is the usual modulus of continuity defined by

$$\omega_1(g;\delta) = \sup_{\substack{x,y \in [0,1] \\ |x-y| \leq \delta}} |g(x) - g(y)|, \forall f \in C[0,1].$$

Considering (1) and (2), we can write

$$\left|B_n(f_{\pm}^r; x) - f_{\pm}^r(x) - \frac{1}{2}(f''(x))_{\pm}^r B_n((\cdot - x)^2; x)\right|$$

$$\leq \left|B_n(f_{\pm}^r; x) - f_{\pm}^r(x)\right| + \frac{1}{2}\left\|(f'')_{\pm}^r\right\| |B_n((\cdot - x)^2; x)|$$

$$\leq \frac{3}{2}\omega_1\left(f_{\pm}^r; \frac{1}{\sqrt{n}}\right) + \frac{1}{8n}\left\|(f'')_{\pm}^r\right\|, \tag{3}$$

respect to $\pm$, respectively. Here $\| \quad \|$ denotes the uniform norm on the Banach space $C[0,1]$.

Consequently, considering basic notations of fuzzy numbers, we obtain

$$D\left(B_n^{\mathcal{F}}(f;x), f(x) \oplus \frac{1}{2} B_n((t-x)^2; x) \odot f''(x)\right)$$

$$= D\left(\left[(B_n(f;x))_-^r, (B_n(f;x))_+^r\right], [f_-^r(x), f_+^r(x)] \right.$$

$$\left. + \frac{1}{2} B_n((\cdot - x)^2; x)[(f'')_-^r(x), (f'')_+^r(x)]\right)$$

$$= \sup_{r\in[0,1]} max\left\{\left|B_n(f_-^r;x) - f_-^r(x) - \frac{1}{2}(f''(x))_-^r B_n((\cdot - x)^2;x)\right|, \left|B_n(f_+^r;x) - f_+^r(x) - \frac{1}{2}(f''(x))_+^r B_n((\cdot - x)^2;x)\right|\right\}$$

$$\leq \sup_{r\in[0,1]} max\left\{\frac{3}{2}\omega_1\left(f_-^r;\frac{1}{\sqrt{n}}\right) + \frac{1}{8n}\|(f'')_-^r\|\ ,\ \ \frac{3}{2}\omega_1\left(f_+^r;\frac{1}{\sqrt{n}}\right) + \frac{1}{8n}\|(f'')_+^r\|\right\}$$

$$\leq \frac{3}{2}\sup_{r\in[0,1]} max\left\{\omega_1\left(f_-^r;\frac{1}{\sqrt{n}}\right), \omega_1\left(f_+^r;\frac{1}{\sqrt{n}}\right)\right\}$$

$$+\frac{1}{8n}\sup_{r\in[0,1]} max\{\|(f'')_-^r\|, \|(f'')_+^r\|\}$$

$$= \frac{3}{2} D\left(\omega_1^{\mathcal{F}}\left(f;\frac{1}{\sqrt{n}}\right), \tilde{o}\right) + \frac{1}{8n} D^*(f'', \tilde{0}),$$

which completes the proof.

Conclusion

By Theorem 4, taking into account in Lemma 3 (iv), we obtain

$$\lim_{n\to\infty} \omega_1^{\mathcal{F}}\left(f;\frac{1}{\sqrt{n}}\right) = 0.$$

Therefore

$$\lim_{n\to\infty} D\left(\omega_1^{\mathcal{F}}\left(f;\frac{1}{\sqrt{n}}\right), \tilde{o}\right) = 0.$$

Thus

$$D\left(B_n^{\mathcal{F}}(f;x), f(x)\oplus\frac{1}{2}B_n((t-x)^2;x)\odot f''(x)\right)$$

converges uniformly to zero, which means that $\frac{1}{\sqrt{n}}$ is an approximation degree corresponding fuzzy asymptotic expansions of Voronovskaja type for the fuzzy Bernstein polynomials.

REFERENCES

[1] Anastasiou, G.A., (2010). Fuzzy Mathematics: Approximation Theory. Springer-Verlag, Berlin.

[2] Bernstein, S., (1912). Démonstration du théorème de Weierstrass fondée sur le calcul des probabilities. Comm. Soc. Math. Kharkov.13: 1-2.

[3] Cheney, E.W., Sharma, A., (1964). Bernstein power series. Canad. J. Math. 16: 214-252.

[4] Gal, S.G., (1993). A fuzzy variant of the Weierstrass' approximation theorem. J. Fuzzy Math. 1(4): 865-872.

[5] Gal, S.G., (1995). Approximate selections for fuzzy-set valued mappings and applications. J. Fuzzy Math. 3(4): 941-947.

[6] Gal, S.G., (2000). Approximation theory in fuzzy setting in: G.A. Anastassiou (Ed.), Handbook of Analytic-Computational Methods in Applied Mathematics, Chapman & Hall/CRC, Boca Raton, London, New York, Washington DC: 617—666.

[7] Gal, S.G., (1994). Degree of approximation of fuzzy mappings by fuzzy polynomials. J. Fuzzy Math. 2(4): 847-853.

[8] Goetschel, R., Voxman, W., (1986). Elementary fuzzy calculus. Fuzzy Sets and Systems. 18: 31-43.

[9] Lorentz, G.G., (1953). Bernstein polynomials. University of Toronto Press.

[10] Wu, C., Zengtai, G., (2001). On Henstock integral of fuzzy-number-valued functions Part I. Fuzzy Sets and Systems. 120 (3): 523-532.

[11] Wu, C., Danghang, L., (1999). A fuzzy variant Weierstrass approximation theorem. J. Fuzzy Math. 7(1): 101-104.

[12] Wu, C., Ming, M., (1991). On embedding problem of fuzzy number space Part I. Fuzzy Sets and Systems. 44: 33-38.

[13] Zareh, L.A., (1965). Fuzzy sets. Inform. and Control. 8: 338-353.

Chapter 2

ADVANTAGES OF THE HYPERSPECTRAL SATELLITE MISSIONS IN REMOTE SENSING SCIENCE

Onur ŞATIR[1]

1 Van YYU Faculty of Architecture and Design Dept. of Landscape Architecture osatir@yyu.edu.tr

1. Introduction

Hyperspectral remote sensing can be described to be all systems that are provided remotely sensed data in narrow wavelengths basically. A typical hyperspectral sensor can be recorded the light in a range of 400 – 2500 nm with 20nm sensitivity. However, traditional multispectral sensors can be recorded the reflectance in 100 nm or higher ranges (Thenkabail et al. 2012). High spatial resolution hyperspectral earth observation satellite sensors were started first with Hyperion sensor on EO 1 (Earth Observation 1) platform in 2000s experimentally. Hyperion mission was started by the NASA (Pearlman et al. 2001; Ungar, 2001). Another hyperspectral mission was run by the (European Space Agency) ESA on 22nd October 2001 called CHRIS on PROBA-1 Platform (Satir et al. 2010). Both hyperspectral sensors were samples of the experimental Earth Observation satellite missions.

Nowadays, hyperspectral satellite sensors are served experimentally, and they are provided vital information to planned hyperspectral missions. So they have some limited abilities such as scanning width, signal noise, mid-special resolution and periodic data transfer.

There have been many studies on plant ecology, physical analyses, and mining in the literature until today. In general, most of the researches that were used hyperspectral satellite sensors were given more accurate results than multispectral studies. For example, according to the Bannari et al. (2006), was 10% more accurate results than multispectral dataset was obtained usingone time hyperspectral dataset on crop pattern mapping and harvest prediction.

Hyperspectral satellites are provided detailed information on plant nutrients, plant water content, pigment and protein content, chlorophyll content, light use efficiency (LUE) soil moisture, Soil organic carbon, main rock type, ground mineral content, water pollution and surface rock and soil materials. The purpose of the paper is to compare future and current hyperspectral satellite sensors to detect the future contribution of the hyperspectral satellites on soil, plant, water and mining researches.

2. Space Borne Hyperspectral Technologies from Past to Future

Two Hyperspectral experimental satellite sensors have been used widely until today. Hyperion and CHRIS PROBA are two frontiers on hyperspectral earth observation in high and mid spatial resolutions. Additionally, there are some hyperspectral satellite sensors that are used on global scale studies such as HICO, OMI and SCIAMACHI.

The first high resolution hyperspectral satellite has been Hyperion, and it started to provide data in 2000s. This mission was the break point to see the hyperspectral satellite capabilities and problems in application in high spatial and spectral resolution. In addition to high spatial resolution missions, some of the hyperspectral satellite sensors were developed for observing atmosphere, water and environmental variables in global scale.

Today, countries, which are wanted to be frontier in space, have been developed new space borne hyperspectral sensors for commercial and scientific requirements.Only high spectral resolution are not enough to obtain detailed information from the earth surface. Therefore, researches are tried to combine both spatial and spectral abilities in one platform. Particularly, planned missions are focussed on the requirements on spatial resolutions. Also this type of the space borne sensors called 2nd generation hyperspectral satellites. Active and planned space borne hyperspectral sensors are shown in table 1. Planned missions have been adapted from Transon et al. (2018).

HyspIRI and HypXIM planned missions are different from other planned missions on spectral and spatial resolutions. When the HyspIRI mission will have been lunched, it will be the first space borne hyperspectral mission in thermal wavelength. HypXIM is stand out its spatial resolution (8m) (Table 1).

Table 1. Active and planned hyperspectral space borne sensors until 2019

Sensor/ Platform/ Country	Spatial Res.	Spectral Res.	Spectral range (nm)	Swath Width	Expected Lunch Date
Active Space borne Hyperspectral Sensors					
HICO/ISS/USA	90m	128	353 – 1080	42km	2009 - Current
OMI/Aura/USA	13X12km	740	270 – 500	145km	2004 - Current
SCIAMACHI/ ENVISAT/ESA-EU	30X60km	~2000	212 – 2384	960km	2002 - Current
Hyperion/EO-1/ USA	30m	220 (196*)	427 – 2395	7.5km	2000 - Current
CHRIS/PROBA/ ESA**	17 – 34m	19 - 64	200 – 1050	17.5km	2001 - Current
Taingong-1/ Shenzhou-8 / China	10 – 20m	128	400 – 2500	10km	2001 - Current
Planned Space borne Hyperspectral Sensors					
HyspIRI/USA	30 - 60m	214	380 – 12000	145 - 600km	2020-2021
EnMap/Germany	30m	92	420 – 2450	30km	2020-2021
PRISMA/Italy	30m	250	400 – 2500	30km	2020-2022
HISUI/Japan	20 - 30m	186	400 – 2500	20km	January 2020
HypXIM/France	8m	210	400 – 2500	15km	unknown
SHALOM/Israel-Italy	10 - 20m	275	400 – 2500	30km	unknown

** 196 wavebands calibrated,*
*** Spectral and spatial resolutions are different based on products.*

3. Studies Using Hyperspectral Space Borne Sensors on Plant and Minerals

There are many studies on hyperspectral remote sensing in the literature. In this study, only space borne sensors were considered, and plant, soil, agriculture and mineralogical studies were filtered. More than 200 papers were selected using Web of Science (WOS), Scopus and specific hyperspectral workshop proceedings from 2007 to September 2019. Subjects of the papers were divided according to the paper content, material and methodology. Twenty one specific subjects were defined, and all papers were categorized based on subjects.

Space borne hyperspectral sensors were used on detailed vegetation and crop mapping widely. Studies were concentrated 400 – 2500nm because of sensor specifications. This wavelength range was very important on vegetation and water studies. Therefore, the papers were about on these subjects generally. When multispectral mapping studies were focussed on general Land Use Cover (LUC), hyperspectral mapping studies were about detailed LUC in species scale (level 3 – 4 in CORINE and Anderson). Additionally, accuracy of the maps were higher than multispectral studies significantly (Bannari et al. 2006; Laurin et al. 2016). Hyperspectral space borne sensors are opened a new gate to the vegetation and mineral indices. Laboratory based spectrometer studies are applied to the earth observation because of narrow range detection ability of the space borne hyperspectral sensors. Particularly, vegetation, soil and mineral detection indices were started to use in wide areas to quantify the ecosystem services.

Table 2. 2007 – September 2019 Space borne Hyperspectral Papers in literature on plant, soil and mineral detection

Subject	Total article	Percent
Crop monitoring and pattern mapping	19	8.8%
Vegetation indices	18	8.3%
Detailed vegetation mapping	17	7.9%
Soil chemical properties	17	7.9%
Plant nutrient detection	16	7.4%
Reviews on agricultural subjects	14	6.5%
Comparisons of hyper-multi spectral	14	6.5%
Plant water stress and quantities	12	5.5%
Plant chlorophyllcontent	12	5.5%
Mineral detection	12	5.5%
NPP and crop harvest prediction	11	5.1%
Precision agriculture	9	4.2%
Leaf area index	8	3.6%
Crop and timber biomass detection	8	3.6%
Soil Organic Carbon studies	8	3.6%
Plant diseases detection	5	2.3%
Aridity risk detection	4	1.8%
Soil salinity detection	4	1.8%
Soil and water heavy metal content	3	1.4%
Soil moisture	3	1.4%
Light use efficiency	3	1.4%
Total	**217**	**100%**

When we compared the multispectral, hyperspectral space borne and air borne hyperspectral researches, it was clearly shown that hyperspectral space borne studies have been shined with narrow wavelength recording ability with appropriate swath width and cost from all other sensors. Though hyperspectral air borne UAV technologies are developed, hyperspectral cameras are still too expensive, and periodic data obtaining is harder than space borne sensors. In general, basic advantages and disadvantages of the space borne, air borne hyperspectral and space borne multispectral sensors were focussed on table 3.

Table 3. *Comparisons of the multi-spectral, hyperspectral space borne and hyperspectral air borne sensors in general based on literature*

Subjects	Multispectral Space borne	Hyperspectral Air borne	Hyperspectral Space borne
Image pre-processing time	***	*	**
Swath width	***	*	**
Spectral resolution	*	***	***
Spatial resolution	**	***	*
Time resolution	***	*	**
Image classification accuracy (in equal conditions; same level and method etc…)	**	***	***
Related article counts	***	**	*
Image cost	***	*	***
Total mark	20	15	17

*(*** stars and * star refer the most appropriate and the poorest performances respectively)*

4. Conclusion

According to the table 3, hyperspectral space borne sensors were got the lower mark than multispectral sensor studies because of lack of the articles and spatial resolutions. Planned hyperspectral missions will address this gap over time. Also multispectral space borne sensors will lose importance in the future. Only archive can be kept the importance on multispectral sensors. Another important problem with hyperspectral data is big data processing time. Particularly, multi temporal hyperspectral datasets are included many wavebands. This is a temporary problem because computer technologies are developed fast, and new image pre-processing and classification softwares and codes have been developed.

There are many hyperspectral space borne studies on image classification, crop and vegetation monitoring, soil and plant chemical components, and reviews of hyperspectral sensors. However, there are lack of studies about soil and water pollution, soil salinity, aridity and plant light use efficiency (Table 2).

Hyperspectral air borne sensors were used mining studies widely instead of space borne hyperspectral sensors because of lack of the hyperspectral satellite and spatial resolution. On the other hand, new space borne sensors will probably use very efficiently in mining studies covering big areas in the future.

REFERENCES

Bannari, A., Pacheco, K., Staenz, H., McNairn, K. Omari., 2006. Estimating and mapping crop residues cover on agricultural lands using hyperspectral and IKONOS data, Remote Sensing of Environment, 104, 447-459.

Laurin, G.V., Puletti, N., Hawthorne, W., Liesenberg, V., Corona et al. 2016. Discrimination of tropical forest types, dominant species, and mapping of functional guilds by hyperspectral and simulated multispectral Sentinel-2 data, Remote Sensing of Environment, 176, 163 – 176.

Pearlman, J.,Carman, S., Segal, C., Jarecke, P., andBarry, P., 2001. Overview of the Hyperionimagingspectrometerfor the NASA EO-1 mission," in *Proc. IGARSS*, Sydney, Australia.

Şatir, O., Berberoglu, S., Kapur, S., Nagano, T., Erdoğan, M.A., Dönmez C., et al., 2010. Soil Salinity Mapping Using CHRIS PROBA Hyperspectral Data", ESA Hyperspectral workshop 2010, Frascati, ITALY, CD.683.

Thenkabail, P.S., Lyon, J.G., Huete A. 2012. Hyperspectral Remote Sensing of Vegetation, CRC Press.

Transon, J., d'Andrimont, R., Maugnard, A., Defourny, P. 2018. Survey of Hyperspectral Earth ObservationApplications from Space in the Sentinel-2 Context, *Remote sensing,* 10: 157.

Chapter 3

ENGINEERING PYHSICAL RELIABILITY ANALYSIS OF NEW UNMANNED AERIAL VEHICLES (UAVS) FORSTRESS, STRAIN, DEFORMATION COMPUTATIONAL STUDY IN INTEGRATED CFD PRESSURE-VELOCITY-ACOUSTIC AND STRUCTURAL DESIGN

Özdoğan KARAÇALI[1]

1 Associated Professor Dr., Department of Mechanical Engineering,Engineering faculty,İstanbul University-Cerrahpaşa, Avcılar, Istanbul, 34320 Turkey,ozdogank@istanbul.edu.tr

1. Introduction

The fastest ways of transportation without pilotless, the plane UAV is becoming more popular than the last two decades. This popularity led to research exploring aiming to develop safer and faster UAVs [1]. It should be extremely useful for the search for vehicles based on CFD analysis and numerical methods and for aerodynamic research on airplanes. UAVs are used for coastal surveillance, weather observations, forest fire monitoring, scientific data collectionfor military and various civilian facilities [2]. The UAV pilotless aircraft system is the communication medium between the open pilot control systems. UAV frame, wing, mainframe propeller, engine and battery, electronic sensors, frame design has emerged as a result.

In the study, integrated CFD and structural design analysis of an Unmanned Aerial Vehicle (UAV), which was prepared as a finite element model as a whole, was performed; finite element analysis properties were obtained. Aerodynamics is a mechanistic field that examines the forces and moments necessary for sustainable motion in the air. Aerodynamic forces acting on flying objects are called lifts in flight direction [3].The model used in the study is 5.23 m. length, 6.04 m. is a UAV model with a wing opening, two motors, one at the front and one at the rear, and two vertical stabilizers are fastened with reinforced tubular connection. Composite, wood and aluminum are used as production materials in various parts of UAV. In this study, 3D UAV model developed as shown the SOLIDWORKS- solid model of the UAV in Figure 1.To calculate aircraft clearance pressures, a CFD model of the UAV has been described in further sections. ANSYS CFD flow was modeled.Next section provides literature review OF UAV developed and analyzed in this research.

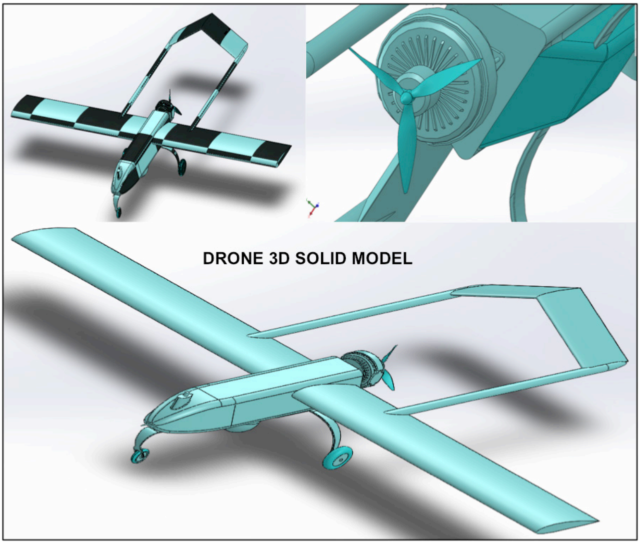

Figure 1The drone-3D model

2. Literature Survey

Unmanned aerial drones (UAVs) produce continuous new formation solutions ranging from small size and mass to similar to pilot aircraft. The main reason for UAV use is due to lower design, realization and operating costs compared to human-piloted aircraft. [4].

Engineers are investigating the impact of acoustic loads on aircraft structures with rising jet engine noise. These high acoustic loads can cause fatigue problems due to acoustic load in aircraft. Various methods have been developed to investigate the effects of acoustic charges [5-7].

The IEA method is R.H. Developed by Lyon [8]. This method examines the power transfer or flow between vibrated structures using the energy balance principle. This method is more widely used in the high frequency region, where geometric changes and material properties are less effective. Techniques such as finite element analysis or boundary element approach known to be sensitive to geometric changes and material properties are inadequate in the high frequency region. Although they are theoretically feasible, they require multiple degrees of freedom to solve simple systems.IEA is very useful in structures by high modal denseness in the high frequency region. In this research, a mixturescheme based on the IEA method and the velocity-strain relationship developed by Karczub and Norton [9] is used to calculate stresses due to acoustic loading.

Two different finite element models have been prepared for aeroelastic analysis. The first one is the structural model that includes wing geometry, material properties and boundary conditions and the other is aero model. The Aero model calculates aerodynamic loads using the Doublet-Lattice subsonic transport surface theory (Ueda & Dowell, 2014). Unlike the structural model, it does not have mechanical properties and consists of surfaces on the same plane. The interaction between the structural model and the aero model is made by means of matrix tools called splines. Splines move the displacement in the structural model to the aero model and the loads in the aero model to the structural model. Thus, the effect of the post-deformation shape of the structure on the aerodynamic forces is included in the analysis. Features and theories of the aero model can be found in detail in the Nastran user guide (Rodden& Johnson, 2013).

Mikhailova [13] developed a finite element method to analyze the landing of a helicopter numerically. Mikhailova et al. [2015] developed three-dimensional design model of a helicopter tubular skid landing gear based on the application of the large beam displacement theory. The analysis of a real helicopter structure was given, that confirms sufficient validity of calculation results, obtained using the model developed by comparing with the numerical and experimental values. Kim et al. have studied the nonlinear crash behavior of the skid landing gear of helicopter. Detailed three-dimensional finite element model with variable thickness and material nonlinearity was constructed for required impact design conditions [16].

Constructive solutions of flying wing UAV are characterized by a series of requirements and exploitation limits on whole cycle of conception, fabrication and testing. UAV requirements and exploitation limits can be grouped on the followingcategories: design concepts, aero-mechanical, materials and technologies, testing methods, flight safety and security and economical [5, 6, 7, 15 and 16].

UAV is used in various civil and military type of mission including reconnaissance surveillance, target tracking and high structure inspection [1]. Furthermore, UAV has also been widely used as experimental platform in various research groups in university to test and validate guidance, navigation, dynamic modeling and control approaches [2-5]. There is no standard to classified unmanned aircraft. However, UAV can be distinguished from one another by size, weight, endurance, range, altitude, mission and design approach.

Active noise control is a complex multi-disciplinary problem that involves fluid dynamics, structural dynamics and control theory, making it a challenge in mechanical engineering. Many solutions to this challenging problem have been proposed. Typically, there are two main strategies for the active control of noise. One is that auxiliary power (secondaryforce) is added directly to the vibrating structure to generate secondary noise that cancels the original noise. This is known as Active Structural Acoustic Control (ASAC) [3,4]. The second control strategy is to focus on directly introducing secondary sound sources to suppress unwanted noise. This is called Active Noise Control (ANC) [5–7] and was first correctly proposed by Lueg [8]. Active structural acoustic control has become increasingly popular because of the development of smart materials and smart structures [1,4,9,10]. Gardonio and Elliott proposed a theoretical study of the active control of noise transmitted through a double panel [11]. Active modal control of the structural-acoustic response of a fluid-loaded plate was implemented by Li [12] using vibration suppression. The negative-velocity feedback control law used in this research was obtained from an uncoupled system. Pinte et al. proposed a design process for the development of an ASAC system that includes the optimization of the location of an actuator/sensor and the design of a control algorithm [13]. For the three-dimensional complex vibro-acoustic problem, Song et al. [14] presented an active modal control system. Through modal analysis, the modes needing control are selected. These are the modes that contribute significantly to the acoustic response. A robust LQG controller was adopted to design the closed-loop system for attenuating the interior noise of a 3-D structure and piezoelectric materials were used as actuators generating secondary noise. A parametric study (including theoretical and experimental components) of the active structural acoustic control of a double-panel system was implemented by James and Fuller [15]. Meurers et al. [16] proposed a model-free frequency-domain iterative active sound and vibration control technology that is suitable for a set of narrow-band noise and vibration modes.

3. Materials and Methods

The geometric design of the main UAV can be divided into four main parts that is fuselage, rudder, horizontal stabilizer and wing. In this study,different conditions of

UAV under the higher load factors were studied that is structural stress, von Mises, shear stress, deformation, pressure-velocity, temperature and acoustic effect on the UAV. In the first condition, structural design issues researched related to material and geometrical properties. In the second condition, aircraft was tested and analyzed to modeled by the pressure and velocity criteria on the plate surface of the UAV. On the thirdsituation, studyof acoustic level was investigated and effects on the surface and mission.

The flight parameters was defined for general characteristics of UAV as 5.23 m in lengths, 1.35 m in height, 6.04 m in wingspan and 251.9 kg in weight. It must be noted that these flight parameters correspond toUAV flight condition. Analysis is performed with the ANSYS CFX solver, according to the turbulence and Navier stroke equation methods for 2100 iterations. In this study an upstream velocity of 1900 m/s & 255m/s is specified at the inlet boundary. All other boundary conditions remain the same as wall. In order to determine the necessary loads, the Mach number, temperature and velocity of the UAV is to be studied and the lift and drag calculation is performed.

In this study, an unmanned aerial vehicle was subjected to simulated loads and the resulting stresses and deformations resulting from these loads were studied in detail. The analyses were carried out in two different stages using both experimental and computational methods. The experimental results, which were obtained by using the data of accelerations, stresses, strains, speeds and the mass, were compared with the results of finite element analysis achieved by using ANSYS LS-DYNA software. Thus it became possible to verify experimental results by the numerical analysis techniques.

In the experimental studies, the examined parameters were the geometric features of the prototype and the kind of material used in the formation of the UAV specimen.

4. ANSYS software: CFD and Finite element analysis

ANSYS offers engineering simulation solution sets in engineering problems that a design process requires. Companies in various industries use this software. ANSYS uses FEM and various other programming algorithms for simulating and optimizing various design problems. ANSYS has many sub parts out of which ANSYS Fluid Flow and Structural are chosen to run the simulations. CFD is applied for analysis of fluid mechanics and dynamics problems. The physical modeling capabilities and the fast, accurate CFD results show that ANSYS Fluent is one of the most comprehensive software for CFD modeling available in the world today.

Finite element method is a numerical solution method that is looking for acceptable precision solution for various engineering problems. Finite element method, which is developed for structural systems, is used in the solution of many engineering problems such as fluid mechanics, ground mechanics, nuclear engineering, electromagnetic fields, and thermal analysis.

Detail design and development of aerodynamic and dimensional wings analysis in the development phase was performed using CFD program. During the flow analysis, firstly the design of the wing was made and freestream was determined. Then, the CFD area is knitted with nets at certain points by finding the unknown; the bearing constant and drag force constants have been obtained. Since the travel speed of the aircraft is 200 m/s, the Mach number is determined as 0.045, and the wing length is calculated as Reynolds number350000. As the flow type is external flow, the turbulence model is used in low Mach and Reynolds numbers as turbulence modeling. As a result of the analysis made in the light of this information, the bearing and drag force values at different attack angles were obtained and compared with the analysis results using ANSYS program.

By examining the effects of airflow on airplane wings and fuselage, CFD research aims to optimize airflow models and provide solutions to aerospace areas for design development and validation of efficient aircraft.

CFD Simulation, also known as CFD modeling, is an engineering-based scientific processing module that works on the theory of Computational Fluid Dynamics to solve problems related to different fluid flows, such as flow rates, density, temperature, and chemical concentrations for any area of flow available. It is a numerical method for nonlinear differential equations that explain depend on fluid flow [aaaa]. CFD simulation is currently being applied in various industries to achieve flawless product design by combining computational tools and fluid dynamics theory. The fundamentals of CFD are the fundamental conservation principles of primitive dynamism, the primitive conservation principle, Newton's second law, and the conservation of energy principle. The finalized finite volume is formulated when numerically adjusted in CFD [4].

To speed up the process, recent advances in CFD tools have made it easier to perform aerodynamic analyzes with the virtual wind tunnel software. The software is a general-purpose finite element solver with predefined turbulence models that helps to quickly evaluate design before prototyping tests.

The finite element method can be applied to the problem in any field: heat transfer, stress analysis, magnetic fields, vibration analysis and so on.There is no geometric limitation. It can be applied to any area of shape.Any loading and boundary conditions may apply. There is no limit to this. Variable and complex material properties within the structure can be applied. Nonlinear, anisotropic and so on.

Compared to prototype tests, finite element analysis costs are lower. Furthermore, the cost, time and better design gains of the finite element method play a major role in the industry's preference for this method. Next section explains the results of the research in the direction of the three condition mentioned above

5. Results

The mock-up geometry was rebuilt with ANSYS starting from SOLIDWORK model as displayed in Figure 2. The mesh was generated with 7.4 millions of hexahedral cells. The grid is refined to properly capture the leading and trailing edge curvature the junction between wing and vertical **empennage**, see Figure 2. The mesh was generated using tetrahedrons element shape. A symmetry plane has been used in this study, in order to reduce the complexity of the solution. To ensure more accurate simulation of the flowfield, it is important to properly size the meshing especially near the wall of the geometry.The received UAV model from SOLIDWORKS to ANSYS is screened for a mesh size of 1.8 mm. The numbers of 2936163 and 639264 are nodes and elements generated correspondingly.

The ANSYS workbench platform provides superior bidirectional connections to all major CAD systems, powerful geometry modification and creation tools with ANSYS Design modeler, advanced meshing technologies in ANSYS meshing as shown in Figure 2. The UAV is meshed at its leading edges like wing, fuselage, horizontal and vertical tail for fine surface mesh size of 2 and mesh scale factor 0.1. And then complete mesh of size 12 and mesh scale factor of 1.A finite volume and density mesh is generated using unstructured tetrahedral cells in the area closely surrounding the aircraft, to allow for the complexities of the geometry, along with a prismatic boundary layer mesh 6 cells thick on the aircraft's wetted surface. In this chapter, due to aerodynamic loading, additional boundary condition was applied as pressure to the skin parts of the hybrid trailing edge control surface. ANSYS automatically maps the aerodynamic mesh on the structural mesh, and transfers the aerodynamic loads to the structural mesh nodes

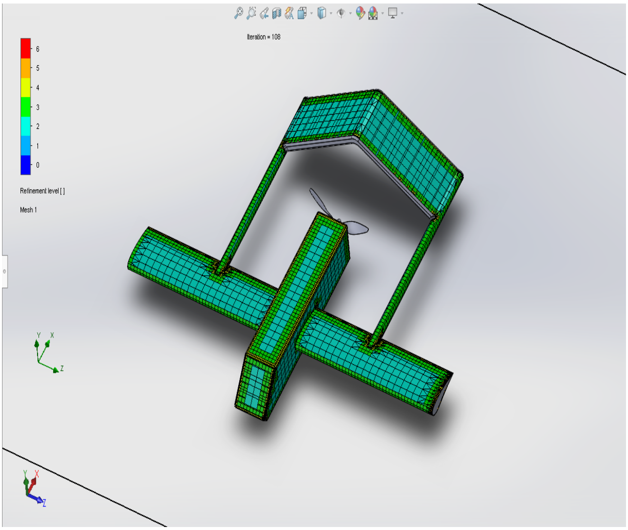

Figure 2 Concept model mesh of the drone

The results obtained from the experiments are given in this section to prove the optimum structural and euro dynamical design of UAV model. It was concluded that the best stress distributions were measured on the fourth landing gear specimen when compared to other specimens. According to the results obtained from the experiments, it was determined that this maximum loading caused concentration of maximum stress distributions at the cutting edges of the stress distribution over the entire structure.The results were evaluated from two perspectives; the first perspective was related with the material surface and its cross sections of UAV and the second one was related with the geometrical shape. Mathematical modeling of the UAV were simulated by successive numerical solutions by using the finite element code ANSYS.

Experimental results have shown that the measured stresses were not in the elastic limits and, as a consequence of this; the design of the landing gear was aimed to perform by using the finite element model optimization. The performed FEA for the optimization of the dimension in terms of UAV model was obtained from different model. In a sense, keeping the design within the elastic limits was achieved by increasing the size. ANSYS analyses were performed according to the given geometrical dimensions. These real values were substituted into the LS-DYN module of ANSYS. Results of application of the FEA model of the stresses generated with loading are presented in Figure 3 as well.

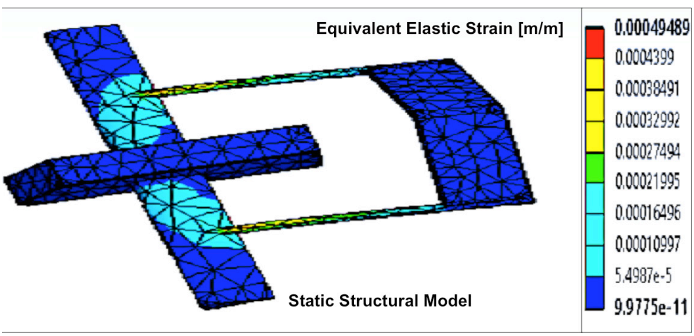

Figure 3 Static structural model analyses for UAV

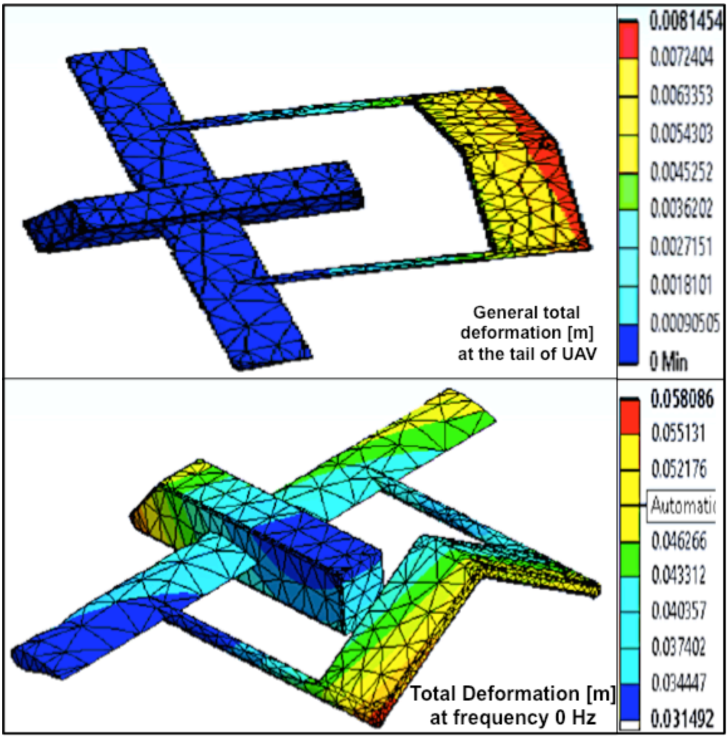

Figure 4Total deformation analyses at the tail of UAV

Numericaland experimental results were verified in terms of stress distributions at the locations where strain caused surface deformation as given in Figure 4.Finite element analysis and experimental results are in agreement with an error of 5.1%. Finally, Finite element model was developed throughout the optimization of dimensions of the fourth specimen and then the obtained force. The 120.3 m/s and 265.17 m/s free flow velocity in the x direction in the initial conditions, 353.64 K temperature and 1 temperature as shown in Figure 5. It shows the drawings and the results of the flow line at different 0.1 and 0.19 Mach numbers.

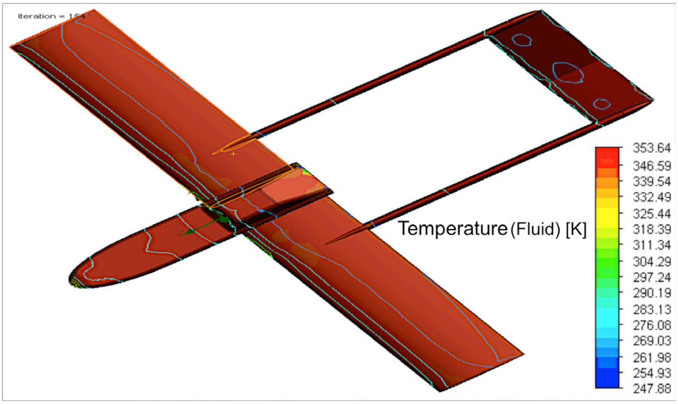

Figure 5 Temperature analysis of UAV surface

The pressure distribution over the wing, and especially over the control surface were sought in order to determine the effects of aerodynamic loads. Additionally, the viscous forces should be taken into account. However, it was seen from the results of the analyses that the viscous forces were very small, and therefore, were neglected during the structural analyses. The obtained pressure distributions were applied to the structural mesh in Finite Element Analyses, and these shear stress distributions are presented in in Figure 6 and Figure 7.

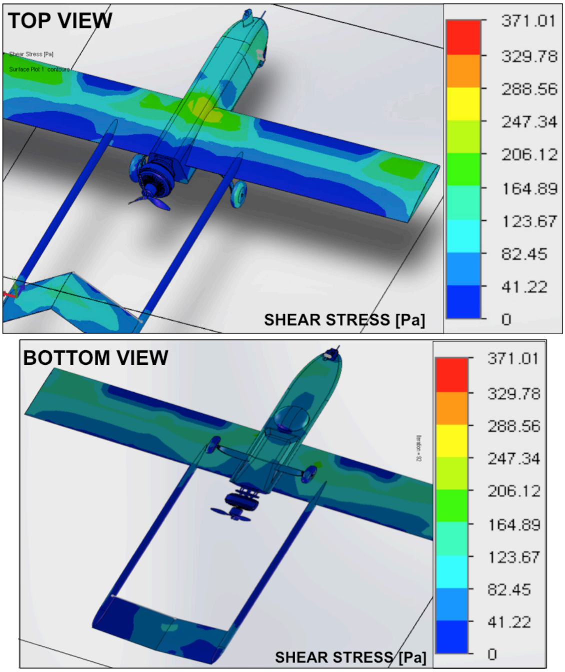

Figure 6 Shear stress analysis of UAV airplane –top and bottom view

In static structural analysis, distortions, fatigue and vibrations, which are the core of the research subject, are total deformation. Von Misses stress criteria, also known as UAV's main body structure-induced stress, shear stress and stress intensity as given in Figure 7.Computing of stress, strain and displacement analysis models were given in Figure 7. To develop the loading structure optimally (i.e. to use the minimal quantity of material) the computational procedure was based on the finite element method (FEM) and its commercial software called ANSYS. The digital geometry was developed in SOLIDWORKS by a specialized module and transferred to ANSYS.

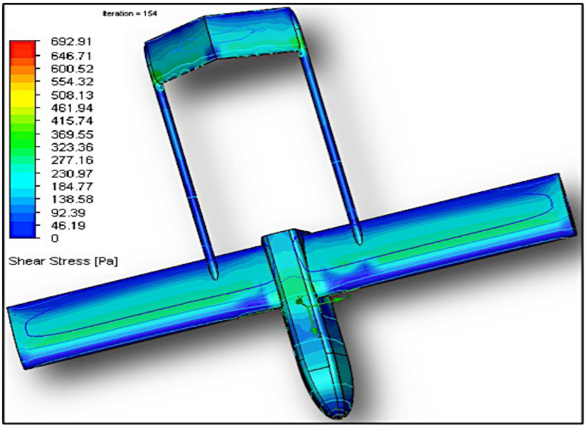

Figure 7 Shear stress analysis of UAV at high altitude

Figure 5 and Figure 6displays the selected results received from ANSYS software. They show external forces, displacements, stress and dividing of considered structure components into finite elements (meshes). Such analyses were performed for mainframe of the body, wing spars, tail beam and tail plane. Normal stress distribution in the poleextensions and the strength of shear stress wing of UAV aircraft was given in Figure 6.Figure 7shows the shear stress on the UAV body and wing using ANSYS Structural.

CFD analysis for a flying wing UAV shows that the aerodynamic optimization is necessary. Furthermore, the CFD results have to be validated with the experimental ones obtained in subsonic wind tunnel as shown in Figure 8. The above analysis shows the aerodynamic characteristics for a flying wing UAV obtained through 3D scan and simplified geometry in junction zones.

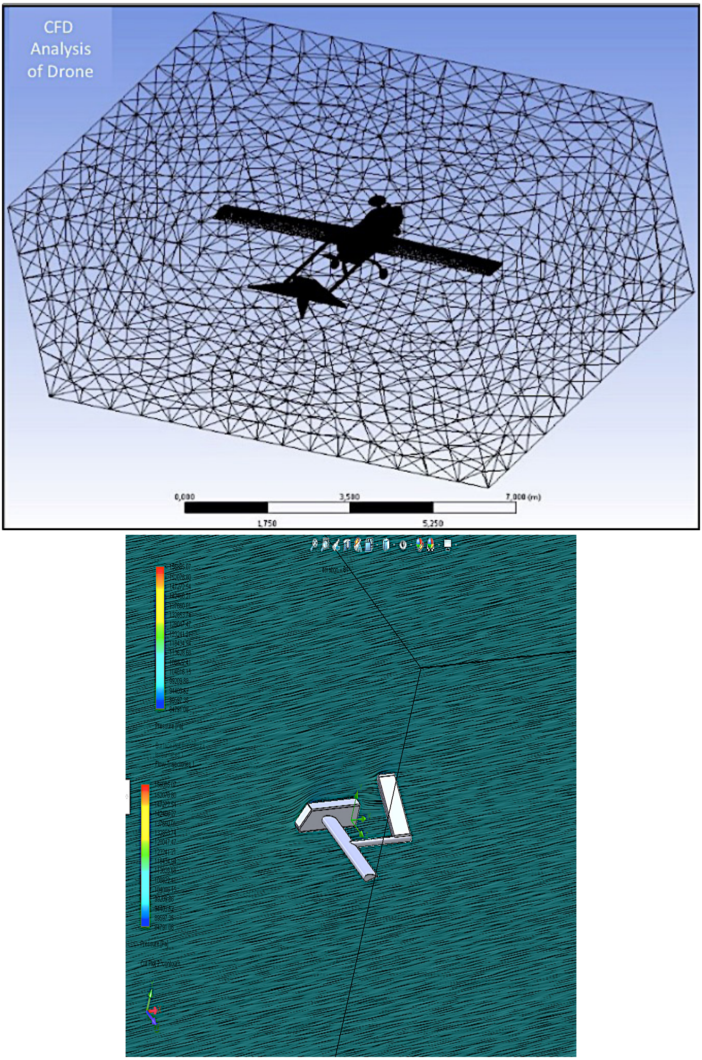

Figure 8 CFD analysis and air velocity with UAV concept in CFD

For a better analysis, it is necessary a finer mesh, which is suitable for UAV computations in ANSYS. Moreover, it is necessary to increase the number of test cases for a velocity range from 0 to 35 m/s and an angle of attack range from -20° to 30°. Computational Fluid Dynamics (CFD) analyses were conducted by using ANSYS software. The CFD simulation requires both configuration file and the mesh file as its inputs. The former input was prepared according to flight parameters, and the latter input was generated directly by Fluent CFD software V19.The flow structures across the UAV help a better understanding of aerodynamics characteristics as shown in Figure 9. This research prove that developing 3-D computational simulation is not only can determine the flow structure, also it can provide aerodynamic performance such as lift, drag and stability in order to meet performance requirement as can be seen in Figure 10.

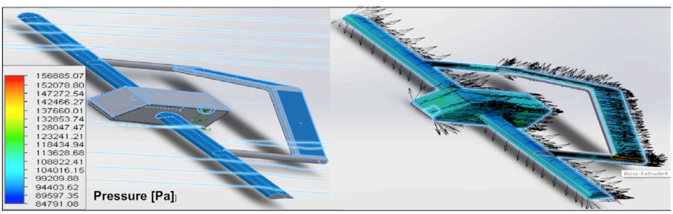

Figure 9 Concept developing with analysis of pressure for UAV

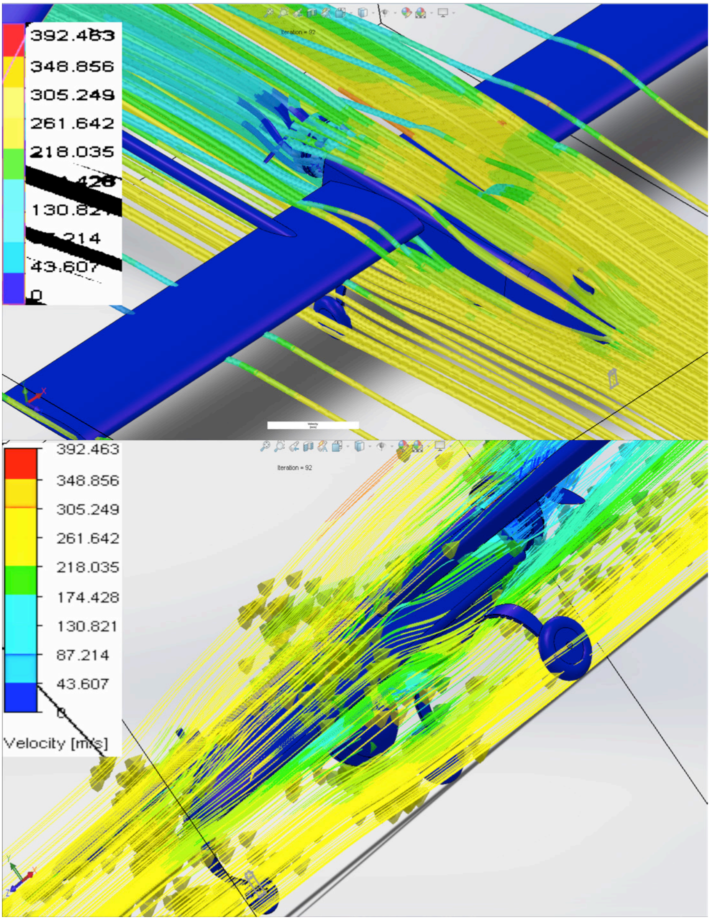

Figure 10 Velocity effect on the drone

The research on dynamics study of UAV is an interesting problems but it is challenging, complex and difficult due to limited study for both theoretical and experimental viewpoints. The purpose of this computational simulation is to evaluate the model's aerodynamic performance and also to enhance stability and performance of the aircraft by Effect of integrated velocity and pressure analysis as demonstrated in Figure 11.

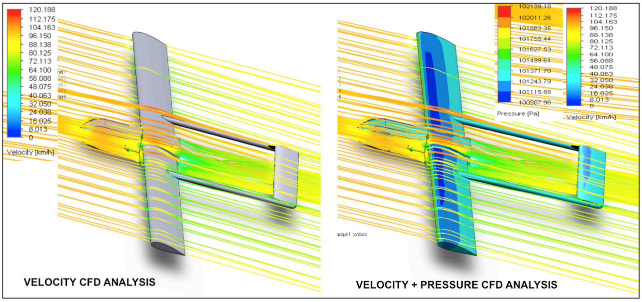

Figure 11 Effect of integrated velocity and pressure analysis

Velocity Distribution Result Figure 11provides a visualization of the airflow around the aircraft and parachute model in order to illustrate details of the structure. When air separate away from aircraft's body surface, its begin to swirl and form turbulent flow resulting in formation of a region of air around aircraft's top surface which has lower velocity and pressure level in Z axis than free stream velocity and pressure as shown in Figure 12.

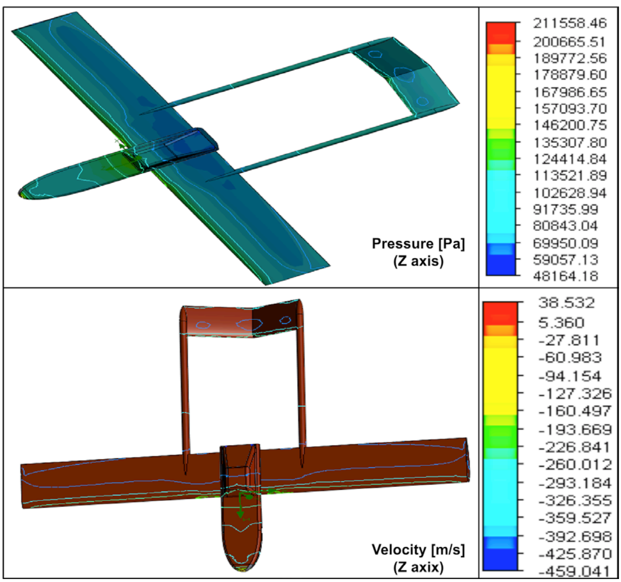

Figure 12 Velocity and pressure analysis in Z axis

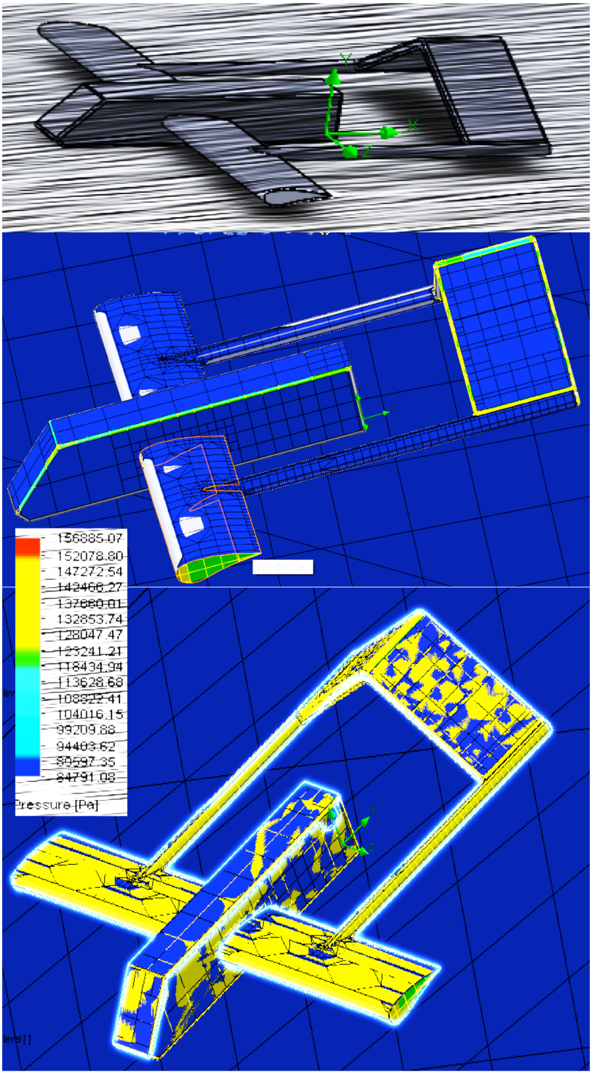

Figure 13 Pressure effect on the surface of model drone

Distribution of pressure on the aircraft is important to study especially to analyze the characteristics of surface concept model as shown in Figure 13. Changes in pressure distribution over the aircraft's body and parachute can be compared between the Figure 13 where slight pressure reduction can be seen. The difference formation of pressure distribution on UAV wing either at the outer or inner surface region can be seen as in Figure 10. High static pressure formed at the inner surface region compared to the static pressure of the free airstream around the UAV due to the formation of turbulent airflow. These difference between inner and outer surface region of the parachute form a strong outwardly pressure that keeps the canopy inflated by Bernoulli's theory from high pressure region to the lower pressure region. The result of this differential pressure, provide an aerodynamic drag for UAV. As UAV moving through air, a vortex form and the air from the below part of the UAV races up.

Some assumptions were made in order to create loading scenarios in the analysis studies. The central points of the front panels are assumed to be 2 meters away from the nose of the aircraft. The center point of the reinforced panel model is therefore 2.75 meters from the nose of the aircraft. It was assumed that the aircraft was traveling at a speed of 200 m/s. In order to apply the turbulent boundary layer, the transport velocity is assumed to be 75% of the free flow rate. Stress levels are assumed to be in the linear region. In this way, Hooke's law can be applied. UAV model developed by ANSYS Software was used in the analysis as shown in Figure 14 and Figure 15. The different loading conditions were examined in the studies. These installation conditions: Apply only turbulent boundary layer condition. In addition to the first loading condition, taking into account radiation emitted from the panels to the outside. Taking into account the car pressurization in addition to the second loading situation 4. Taking account of the noise emitted into the cabin in addition to the third loading situation. When the analyzes are examined, it is seen that the upper frequency limit is determined as 80 kHz. This is a source of error in addition to modal errors in stresses. For the elimination of modal errors, finite element models with very tight network structure can be created to calculate the modal density and to use modal density calculated by the user instead of modal density calculated by ANSYS as modeled in Figure 16.

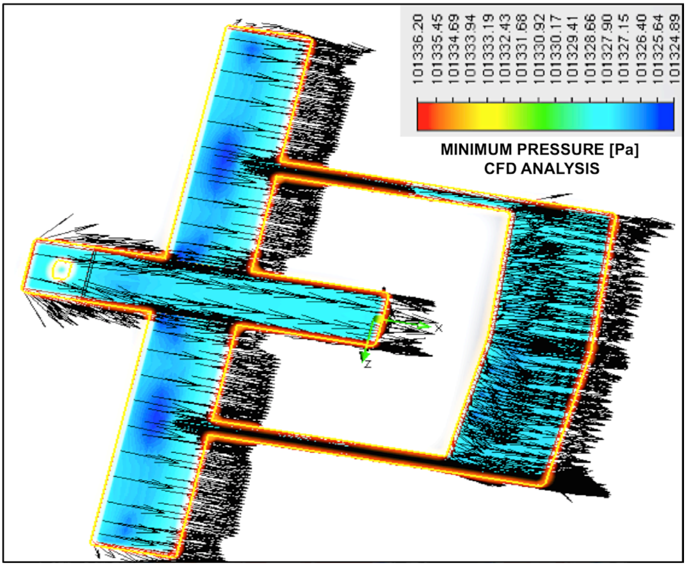

Figure 14Minimum pressure analyses

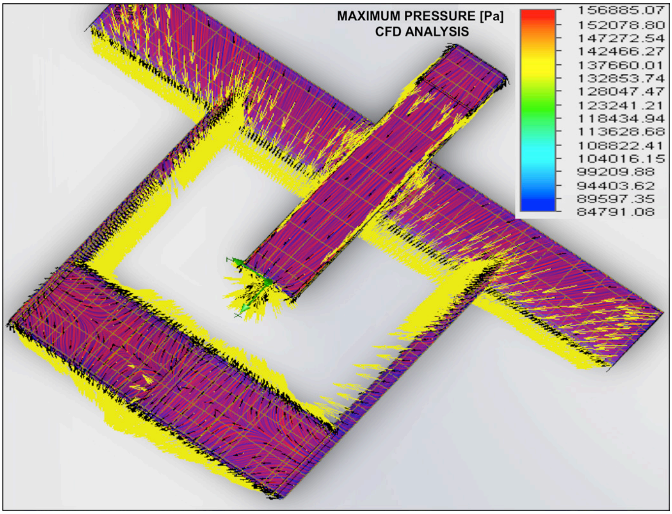

Figure 15Figure maximum pressure analyses

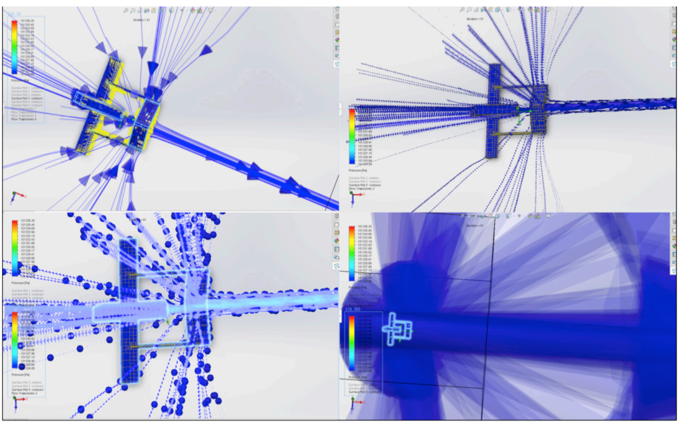

Figure 16Pressure analyses integrated with velocity flow during mission

This research is investigating the impact of acoustic loads on UAV structures with rising engine noise by finite element analysis. These high acoustic loads can cause fatigue problems due to acoustic load in aircraft. Various methods have been developed to investigate the effects of acoustic charges. ANSYS Acoustic software module was employed as a CAE tool allows large acoustic models to be solved as shown in Figure 17.

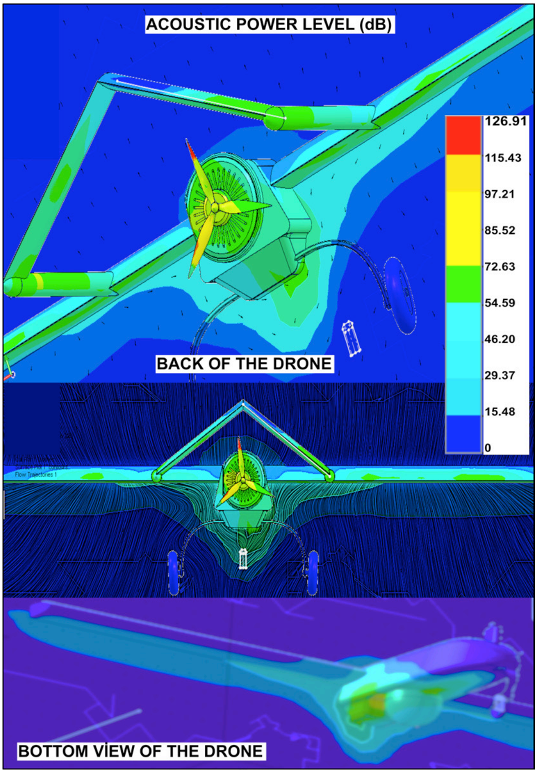

Figure 17Acoustic load analysis of the drone UAVs

The aeroacoustic optimization can increase mismatch in military working conditions, reduce noise pollution in civilian, environmental environments, and allow voice-recording applications. This research was intended to provide a methodology for the design and design of silent and still effective rotors for UAV from aerodynamic estimation, optimization and experimental validation.

The key to the success of the interpretation of finite elements is choosing appropriate interpolations for displacement, pressure and vortex momentum.It provides a fast and reliable solution with finite and infinite elements in its library. With ANSYS acoustics module, the sound fields in the cavities can be defined by a modal or physical approach. Sound absorption walls can be modeled in detail with impedance state or perforated material models. By creating a mean flow field or a temperature gradient, the distribution of sound propagation due to these effects can be examined. Viscose-thermal effects commonly used in the distribution analysis of sound waves in small cavities or channels (such as hearing aids) can also be included in the analysis. Modal results can be obtained from many ANSYS software and can be used as structural models as shown in Figure 18.

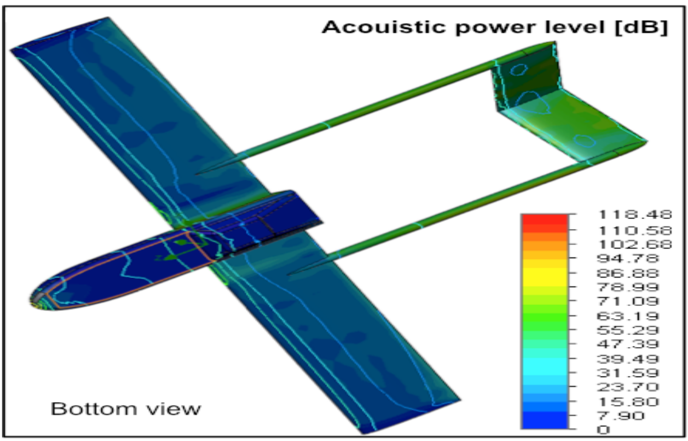

Figure 18 Acoustic power level on bottom surface of the UAV

Acoustic, dynamic and kinematic boundary conditions, as well as turbulent boundary layer or diffuse sound field, which will form a drive on the structure, can be added to the model for more realistic operating conditions as displayed in Figure 18.Acoustic model can solve coupled or uncoupled models in physical or modal coordinates, time or frequency plane. ANSYSaeroacoustics is used to analyze the noise generated by turbulent flow. The program obtains the aerodynamic noise source from commercial CFD programs. ANSYSaeroacoustics program converts CFD results in time plane to frequency plane and interpolates to acoustic solution mesh and obtains solution. Interpolated distribution of results from very small solution networks (usually in the boundary layer) in the acoustic solution network in the ANSYS. Figure 19 and Figure 20 showauroacoustic power level on the front surface andtail-back surface of the UAV.A graph developed acoustic pressure level at frequency 3820 Hz on the surface of UAV is a feature that accelerates the solution time without compromising accuracy as can be seen in Figure 21.

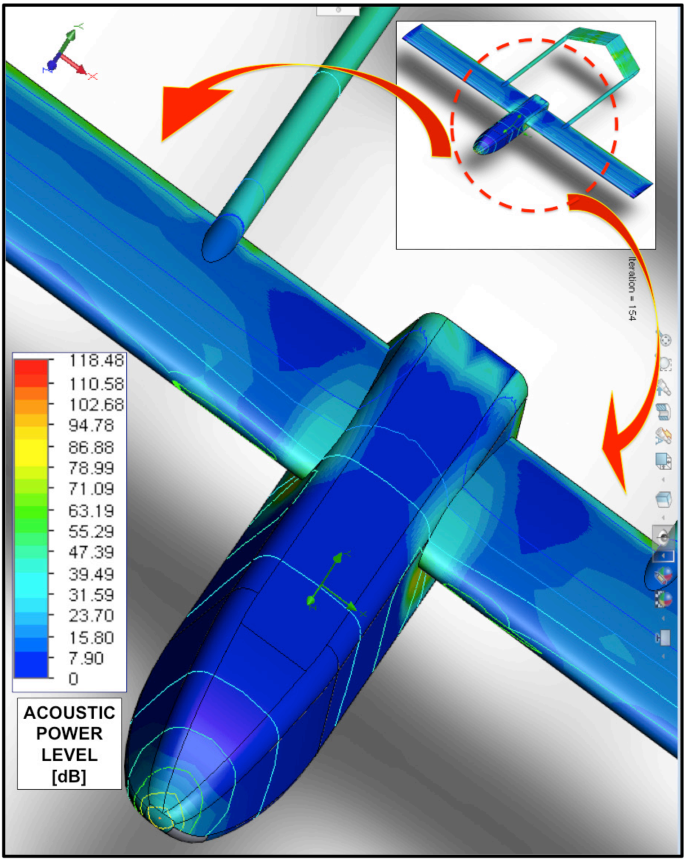

Figure 19Auroacoustic power level on the frontsurface of the UAV

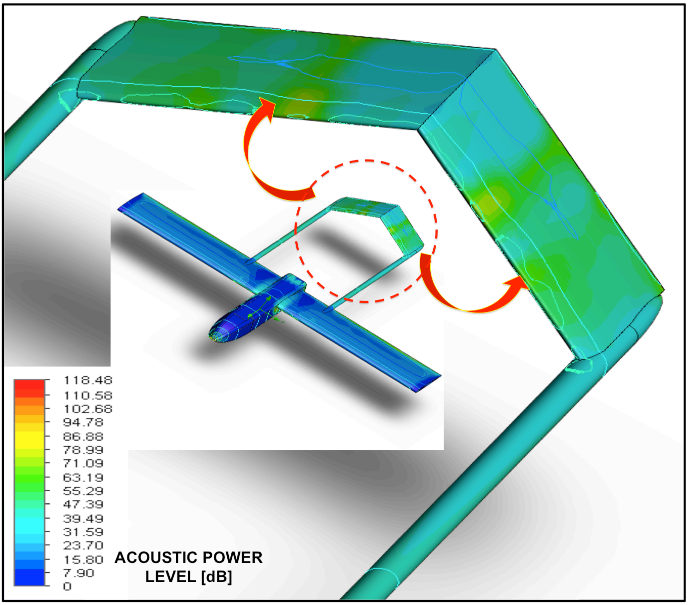

Figure 20 Auroacoustic power level on tail-back surface of the UAV

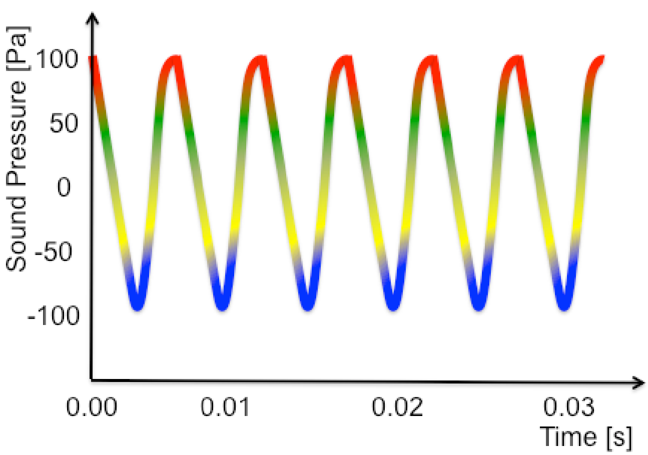

Figure 21 Acoustic pressure level at frequency 118.48 Hz on the surface of UAV

6. Discussions

One of the most important design parameters not only for UAVs but also for any other aircraft is weight of the structure (Goraj et al., 2003; Goraj, 2000a, b). Computer aided design/ manufacture/engineering (CAD/CAM/ CAE) method makes the whole design process easier, shorten the engineering time and in consequence decreases the cost of the project. The range of unmanned aerial aircraft (UAV) is developing continuously generating new constructive solutions from small size and mass to those, which are comparable to piloted aircraft. The main reason of UAV use is due to lower cost of design, realization and operation (on flight hour) in comparison with human piloted aircraft.

This paper presents the CFD analysis on a UAV tailless, after a 3D scanned real model.Hence the proposed analysis method has demonstrated a workable alternative to obtain aerodynamic forces and coefficients by manipulating the results from ANSYS simulation. However, further investigations are suggested in order to reduce the differences in the results at certain conditions, and to enable calculations of friction related lift and drag.

The control surface designs were also analyzed for the cases under the aerodynamic loading. It was shown that both designs are capable of performing both camber and decamber under aerodynamic loading as well.An aeroelastic study can be conducted by combining both structural and aerodynamic properties and a multi-disciplinary optimization of the control surface can also conducted including the producibility factors.Aeroelastic analysis showed that the wing torsional rigidity is not sufficient. To increase the critical flutter speed the wing sandwich skin has been reinforced adding extra layers of carbon fibres. This procedure is iterative by nature, because adding the new layers changes the weight and stiffness of aircraft. Analysis and design methodology is limited to surveillance and monitoring platforms, where the design objectives are long endurance, high reliability and cost effectiveness of the platform.

7. Conclusions

In this study, the computational analyses of the aerodynamic characteristics of UAV were carried out using CFD. The main objective of this analysis was to evaluate the most appropriate design that will improve the aerodynamic performance of UAV. The primary aim of this workwas to investigate the potential loads on different parts of a structure of an aircraft. A review of the literature in this field revealed that very few such studies have been published to date. For this a typical and challenging design was considered and preliminary flow analysis was carried out for the determination of the loads acting on the different parts.From the results the following points can be inferred as material distribution is more where stress is high and material is made void where stress is considerably low. Another conclusion may be all design aspects can be met with minimal material.

In this work, the computational analysis of the aerodynamic properties was researched by integrated CFD and structural design for aerodynamic performance. The main objective of this project is to investigate CFD flow analysis (acoustic level, velocity, pressure causing to stresses and deformations) effect on the surface of the UAV. This research showed that material distribution is more stress and quite low and design features can be met with minimal material under velocity and pressure of air during flying of the UAV.

The results of the verification process, obtained from experimental methods, were taken into account during the numerical simulations, in order to obtain the best design for UAV. Based on this study the following conclusions were reached:A very useful source of design information and patterns was to provide an effective design methodology focused on loading structure of unmanned aerial vehicles. This paper offers practical help for designers planning an unmanned platform to be well adjusted to the assumed mission, giving a lot of practical information about attachments and fittings, on-board systems integrated with loading structure and integration of composites with metal parts in modern flying platforms. A computational simulation study has been performed to determine the aerodynamics characteristics of UAV aircraft.

8. Acknowledgments

This research study was supported by BYP-2019-296392 project by Istanbul University-Cerrahpaşa BAP-scientific research unit.

REFERENCES

Austin R., Unmanned Aircraft Systems – UAVs design, development and deployment, Aerospace series, Wiley and Sons Ltd publication, 2010, ISBN 978-0-470-05819-0, 365p.

He, X.; Bonds, J.; Herbst, A.; Langenakens, J. Recent development of unmanned aerial vehicle for plant protection in East Asia. Int. J. Agric. Biol. Eng. 2017, 10, 18–30.

International Journal of Science and Research (IJSR) ISSN (Online): 2319-7064 Index Copernicus Value (2013): 6.14 | Impact Factor (2014): 5.611 Volume 4

B. Ravi Theja, Dr. M. Satyanarayana Gupta. 'Design and Fluid Flow Analysis of Unmanned Aerial Vehicle (UAV)' Issue 11, November 2015

Beard R W and Mclain T W 2012 Small Unmanned Aircraft; Theory And Practice (New Jersey: Princeton University Press)

Cojocaru, M. G., Niculescu, M. L., &Pricop, M. V. (2015). Aero-Acoustic assessment of installed propellers. INCAS Bulletin,ISSN 2066-8201,7(2), p 53.

Cai G, Chem B M and Lee T H 2011 Unmanned Rotorcraft System (New York: Spriger Publishing Company)

Carneal, J.P., Fuller, C.R. 'An analytical and experimental investigation of active structural acoustic control of noise transmission through double panel systems', Journal of Sound and Vibration 272 (2004) 749–771.

Dowell, E.H., Clark, R., Cox, D., Curtiss Jr., H.C., Edwards, J.W., Hall, K.C., Peters, D.A., Scanlan, R., Simiu, E., Sisto, F. and Strganac, T., "A Modern Course in Aeroelasticity," Kluwer Academic Publishers,2004.

Gardonio, P., 'Review of active techniques for aerospace vibro-acoustic control', Journal of Aircraft 39 (2002) 206–214.

Hodges, D.H. and Pierce, G.A., “Introduction to Structural Dynamics and Aeroelasticity,” Cambridge University Press, 2002.

Wright, J. R., & Cooper, J. E. (2007). Introduction to Aircraft Aeroelasticity and Loads.Johny Wiley& Sons.doi:978-0470-85840-0

Roskam, J., Airplane Design, Lawrence, KS, Design Analysis Research Corporation, 2000.

Prabhakar A. and Ohri A., “CFD Analysis on MAV NACA 2412 Wing in High Lift Take-Off Configuration for Enhanced Lift Generation”, J Aeronaut Aerospace Eng., 2: 125. doi:10.4172/2168-9792.1000125, 2013.

Prisacariu V., Boscoianu M., Cîrciu I., Morphing wing concept for small UAV, APPLIEDMECHANICS AND MATERIALS, Vol. 332 (2013) pp 44-49, ISSN: 1662-7482, © (2013) Trans Tech Publications, Switzerland, doi:10.4028/www.scientific.net /AMM.332.44 OPTIROB 2013.

Karagülle, H., Malgaca, L., Öktem, H.F. ‘Analysis of active vibration control in smart structures by ANSYS’, Smart Materials and Structures 13 (2004) 661.

Karczub DG, Norton MP (2000) Correlations between Dynamic Strain and Velocity in Randomly Excited Plates and Cylindrical Shells with Clamped Boundaries. Journal of Sound and Vibration 230(5): 1069-1101.

Kendoul F 2012 Survey Of Advances In Guidance, Navigation, And Control Of Unmanned Rotorcraft System Journal Of Field Robotics 29 315-378

Lin, Q.R., Liu, Z.X., Wang, Q., ‘Active control of structural acoustic pressure in a rectangular cavity using piezoelectric actuators’, European Journal of

Li, S., ‘Active modal control simulation of vibro-acoustic response of a fluid-loaded plate’, Journal of Sound and Vibration 330 (2011) 5545–5557.

Pinte, G., Boonen, R., Desmet, W., 'Active structural acoustic control of repetitive impact noise', Journal of Sound and Vibration 319 (2009) 768–794.

Raymer, Daniel P. (1999). 'Aircraft Design: A Conceptual Approach' (3rd ed.). Reston, Virginia: American Institute of Aeronautics and Astronautics. ISBN1-56347- 281-3.

Rainald Löhner Applied Computational Fluid Dynamics Techniques: An Introduction Based on Finite Element Methods, Second Edition. © 2008 John Wiley & Sons, Ltd. ISBN: 978-0-470-51907-3

shreyas Krishnamurthy, surajjayashankar, sharath v rao, rochenkrishna t s, shankargoudnyamannavar 'CFD Analysis of An RC Aircraft Wing CFD analysis of an rc aircraft wing' International Journal of Mechanical And Production Engineering, ISSN: 2320-2092, Volume- 2, Issue-9, Sept.-2014

Schubert, F., "Basic principles of acoustic emission tomography,"Journal of Acoustic Emission, vol. 22, pp.147–159, 2004.

Song, C.K., Hwang, J.K., Lee, J.M., 'Active vibration control for structural-acoustic coupling system of a 3-D vehicle cabin model', Journal of Sound andVibration 267 (2003) 851–865.

Tomac, M. and Eller, D., 2011. From geometry to CFD grids—an automated approach for conceptualdesign. Progress in Aerospace Sciences, 47(8), pp.589-596.

Wu JC, Lu XY &Zhuang LX, "Integral force acting on a body due to local flow structures", Journal of Fluid Mechanics, vol. 576, pp. 265-286, 2007.

ACADEMIC STUDIES IN SCIENCE AND MATHEMATICS

gece kitaplığı

www.gecekitapligi.com

/gecekitapligi

/gecekitap

/gecekitapligi

9 786257 912136